Geomechanics and Engineering, *Vol. 11, No. 1 (2016) 141-160*
DOI: http://dx.doi.org/10.12989/gae.2016.11.1.141

Comparative field tests on uplift behavior of straight-sided and belled shafts in loess under an arid environment

Zeng-zhen Qian [1a], Xian-long Lu [*2], Wen-zhi Yang [2b] and Qiang Cui [2c]

[1] *School of Engineering and Technology, China University of Geosciences, No. 29 Xueyuan Road, Haidian District, Beijing, 100083, China*
[2] *China Electric Power Research Institute, No. 15, Xiaoying East Road, Haidian District, Beijing, 100192, China*

(*Received April 24, 2015, Revised February 21, 2016, Accepted April 11, 2016*)

Abstract. This study elucidates the uplift behaviors of the straight-sided and belled shafts. The field uplift load tests were carried out on 18 straight-sided and 15 belled shafts at the three collapsible loess sites under an arid environment on the Loess Plateau in Northwest China. Both the site conditions and the load tests were documented comprehensively. In general, the uplift load–displacement curves of the straight-sided and belled shafts approximately exhibited an initial linear, a curvilinear transition, and a final linear region, but did not provide a well defined peak or asymptotic value of the load, and therefore their uplift resistances should be interpreted from the load test results using an appropriate criterion. Nine representative uplift resistance interpretation criteria were used to define the "interpreted failure load" for each of the load tests, and all of these interpreted uplift resistances were normalized by the failure threshold, T_{L2}, obtained using the L_1-L_2 method. These load test data were compared statistically and graphically. For the straight-sided and belled shafts, the normalized uplift load–displacement curves were respectively established by the plots that related the mean interpreted uplift resistance ratio against the mean displacement at the corresponding interpreted criteria, and the comparisons of the normalized load–displacement curves were made. Specific recommendations for the designs of uplift belled and straight-sided shafts in the loess were given, in terms of both capacity and displacement.

Keywords: loess; pullout testing; straight-sided shafts; belled shafts; transmission tower; load test; ultimate load

1. Introduction

Loess is a wind-deposited soil found in many parts of the world; however, China possesses some of the largest deposits on Earth. The aeolian silt accumulation comprising the Loess Plateau of Northwest China approaches a thicknesses of more than 250 m in the Lanzhou region (Derbyshire *et al*. 1995, Yuan and Wang 2009). The construction of electrical transmission systems connecting West and East China has been planned in recent years. Thus, the construction of

*Corresponding author, Ph.D., E-mail: luxianlong@163.com
[a] Ph.D., E-mail: zzqian@cugb.edu.cn
[b] M.Sc., Civil Engineer, E-mail: yangwenzhi@epri.sgcc.com.cn
[c] Ph.D., E-mail: cuiqiang@epri.sgcc.com.cn

http://www.techno-press.org/?journal=gae&subpage=7 ISSN: 2005-307X (Print), 2092-6219 (Online)

foundations in the loess for transmission towers is unavoidable (Qian *et al*. 2014a). Uplift loading often controls the design of the transmission line foundations (Kulhawy *et al*. 1983). Straight-sided and belled shafts have been recently utilized in the loess to satisfy the axial uplift resistance requirements for the transmission towers. In general, in the design of foundations under an axial uplift loading, the overall uplift load–displacement behavior plays an important role, first in estimating the displacement at a given load, and second in interpreting the failure load or uplift resistance. Therefore, it is essential to characterize the uplift load–displacement behavior and the axial uplift resistance evaluation for both straight-sided and belled shafts in the loess. However, the uplift behaviors for straight-sided and belled shafts in the loess are not well understood, and systematic full-scale pullout tests have not been conducted.

The load–displacement response of an uplift-loaded foundation will depend on the soil property, foundation type, and construction method. By applying representative uplift interpretation criteria, researchers have performed extensive evaluations on the uplift load–displacement responses for drilled shafts in non-gravelly soils (Chen *et al*. 2008), gravelly soils (Chen 2004, Chen and Chu 2012), and Gobi gravel soils (Qian *et al*. 2014b). However, loess is a clastic soil mainly composed of silt-sized quartz particles and loosely arranged grains of sandy, silty, and clayey soils (Gao 1988). Most of the grains are coated with either a thin film of clay or a mixture of calcite and clay. Cohesion occurs when the clay or calcite bonds between particles, which would be significantly weakened under saturated conditions. These soil properties may give rise to a different uplift performance for foundations to be installed in the loess. Therefore, it is of particular interest to examine the criteria and the procedures for assessing uplift load test results of the straight-sided and belled shafts in the loess.

In this study, the comparative field uplift tests on 18 straight-sided and 15 belled shafts were carried out at the three collapsible loess sites in Gansu Province, a typical region of the Loess Plateau in Northwest China. The site geotechnical conditions and the load tests were documented comprehensively. The load test data were interpreted using nine representative uplift resistance interpretation criteria to define various “interpreted failure load” for each of the load tests. These results were compared statistically and graphically, and the recommendations were suggested for the designs of uplift belled and straight-sided shafts in the loess in terms of both capacity and displacement.

2. Test sites and loess properties

2.1 Site description and samples preparation

The comparative field tests on the straight-sided and belled shafts were carried out at the three sites of Gangu County (GC), Dingxi City (DC), and Yuzhong County (YC), along the 750-kV Lanzhou-Tianshui-Baoji transmission line near Lanzhou, the capital city of Gansu province. These three sites are located in the western Chinese Loess Plateau, which is well-known for thick loess terrain in terms of geology. The loess thickness around Lanzhou generally exceeds 30 to 50 m with the maximum record of up to 335 m (Derbyshire *et al*. 1995, Wen and Yan 2014), and the soil can be called as Q_3 loess (late Quaternary loess), also known as “Malan Loess” in China (Liang *et al*. 2014, Xu *et al*. 2014).

To determine the soil properties, a series of laboratory and in-situ tests were performed, including specific gravity, moisture content, unit weight, Atterberg limits, grain size distribution, microstructure, granular components, shear strength, and collapse index. The undisturbed samples of the loess for laboratory tests of each site were obtained by means of block sampling (300 mm × 300 mm × 150 mm blocks), and they were carefully trimmed and waxed from the bottom of a newly excavated 1.2-m-diameter pit at intervals of approximately 1.0 m in the soil profile from 0.4 m to 8.7 m.

2.2 Typical physical index values

Fig. 1 shows the laboratory-measured specific gravity, moisture content, and unit weight for the soil profile at the three test sites. The specific gravities as shown in Fig. 1(a) were found to range from 2.60 to 2.89; the average was 2.79, 2.72, and 2.70 for GC, DC, and YC, respectively, which is similar to the mean specific gravity values for loess in many other parts of the world. For example, specific gravity values for the loess in Algeria are between 2.68 and 2.73 (Nouaouria *et al*. 2008), whereas those for the loess in Libya range from 2.66 to 2.73 (Assallay *et al*. 1996). As may be seen from Fig. 1(b), the moisture contents were found to increase with depth and to range from 3.7% to 12.7%.

The plasticity characteristics of the loess were determined by the Atterberg limits tests, including liquid limit, plastic limit, and plastic index, as summarized in Table 1. The particle size distribution curves of the loess at the three test sites were obtained by sieve and hydrometer analysis tests according to ASTM D422 (ASTM 2007), as shown in Fig. 2.

Based on the Casagrande Plasticity Chart and the provided Atterberg limits in Table 1, the loess can be categorized as CL-ML according to Unified Soil Classification System ASTM D2487-11 (ASTM 2011a). In general, the typical physical index values of loess at the three sites are similar to those reported by Hwang *et al*. (2000) and Ryashchenko *et al*. (2008).

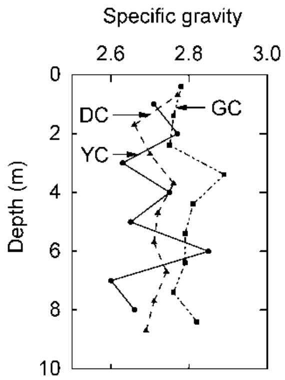

(a) Specific gravity

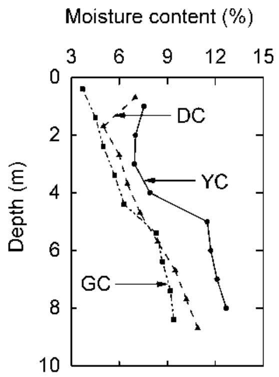

(b) Moisture content

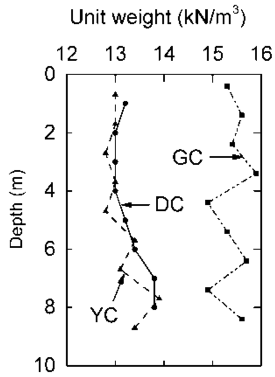

(c) Unit weight

Fig. 1 Laboratory-measured results for the soil profile

Table 1 Atterberg limits test results

Atterberg limits	GC	DC	YC
Liquid limit, LL (%)	28.9	32.6	39.8
Plastic limit, PL (%)	10.8	18.1	21.3
Plastic index, PI (%)	18.1	14.5	18.5

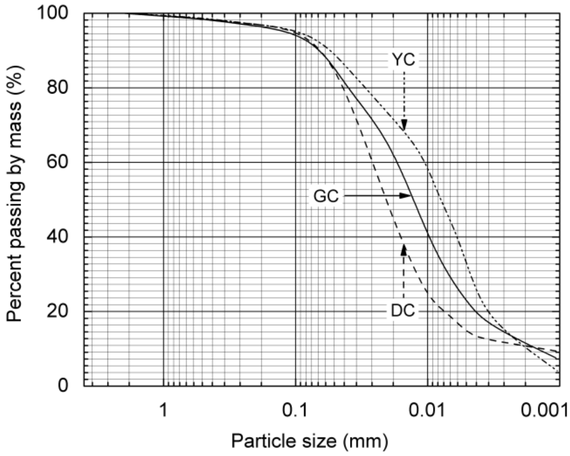

Fig. 2 Cumulative particle-size plot of the loess

2.3 Shear strength

At the sites of GC and YC, the direct shear tests were conducted on the in-situ loess soil. The distances between the predetermined shear plane and the ground surface were 0.4 m, 0.8 m, and 1.2 m for GC, and 0.9 m, 1.5 m, and 2.0 m for YC, respectively. However, at the site of DC, the direct shear tests were conducted in laboratory on the undisturbed samples obtained by means of block sampling in the soil profile.

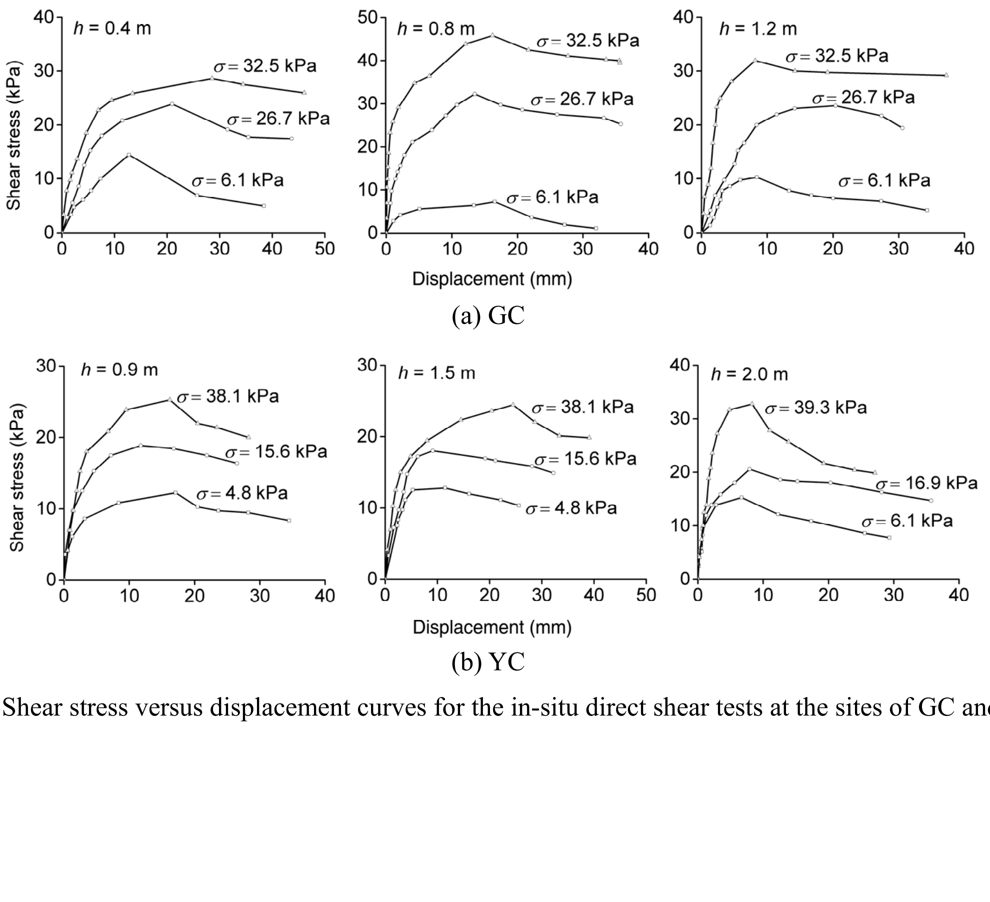

Fig. 3 Shear stress versus displacement curves for the in-situ direct shear tests at the sites of GC and YC

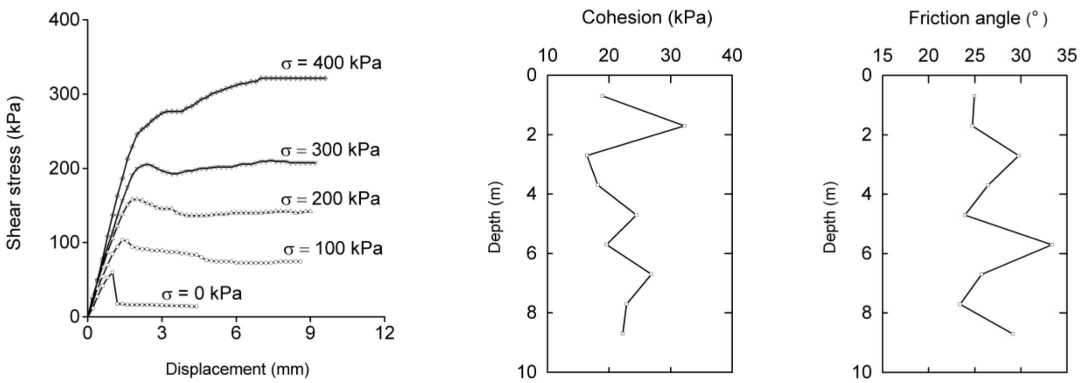

(a) Typical shear stress versus displacement (b) Cohesion (c) Friction angle

Fig. 4 Laboratory shear test results at the site of DC

Standard loading and measuring procedures were conducted for all shear strength tests in accordance with the ASTM D3080 (ASTM 2011b). Fig. 3 shows the shear stress versus shear displacement curves for the in-situ tests at the sites of GC and YC, and Fig. 4(a) shows the typical curves of the shear stress versus shear displacement for a group of the loess soil specimens for the site of DC. All the curves in Figs. 3 and 4(a) show a gradual rise and drop before and after the peak stress, followed by an almost constant residual strength. For the specimens of each group, the peak shear stress was plotted against the normal stress, and a straight line fit was used to determine the fitting parameters of cohesion and friction angle.

According to in-situ direct shear test results in Fig. 3, the typical ranges of the cohesion and the friction angle were 14.8-15.6 kPa, 22.6-23.8°, and 12.4-14.2 kPa, 27.5-38.2° for the sites of GC and YC, respectively. Figs. 4(b) and 4(c) plot the cohesion and the friction angle of loess with depth at the site of DC. A crust layer was found at about 2 m below the ground surface. The cohesion of the loess below the crust layer was found to fluctuate with the depth between 16.4 kPa and 26.9 kPa with an average of approximately 21.5 kPa, and the friction angle fluctuated with depth and ranged from 23.4° to 33.4°, with an average of approximately 27.5°.

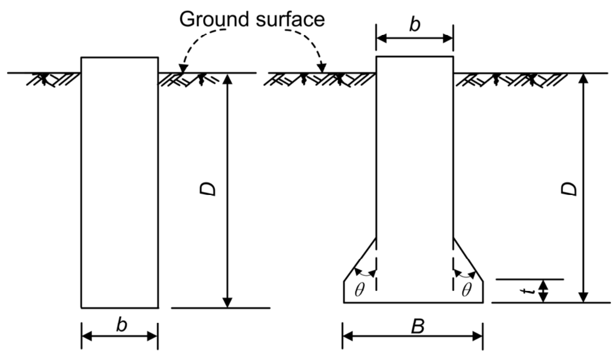

(a) Straight-sided sahft (b) Beleed shaft

Fig. 5 Geometries of straight-sided and belled shafts

3. Foundation installation

To properly utilize the high bearing capacity of loess while avoiding the soil collapse, tower locations would be carefully selected to divert water from the foundations thus maintaining a very dry environment in the loess surrounding the tower foundations. In this study, at the three sites of GC, DC, and YC, a total of 18 straight-sided and 15 belled shafts were installed and tested under a very dry environment. Fig. 5 presents the geometric symbols of the straight-sided and belled shafts, where D is the length from the ground surface to the bottom of the foundation, b is the shaft diameter, B is the bell diameter, t is the toe height of the bell, and θ is the angle created by the pyramidal surface against the vertical for the belled shafts.

Tables 2 and 3 summarize the dimensions for the straight-sided and belled shafts, respectively. In this study, the toe height t was equal to 0.20 m for all of the belled shafts, and the magnitude of angle θ for each belled shaft was equal to or less than 45° so that the unreinforced concrete bell would be sufficiently stiff to withstand the shear stress developed by the uplift loading.

The installation of the straight-sided and belled shafts mainly consisted of manually excavating the hole to the required dimensions and casting the reinforced concrete foundation. However, the construction for a belled shaft was performed by two steps. The first step was to excavate the shaft

Table 2 Dimensions and interpreted uplift resistances for the straight-sided shafts

Site	Shaft No.	Shaft (m)		Interpreted uplift resistance, T [a] (kN)									
		D	b	T_{L1}	T_{DB}	T_{DA}	T_{ST}	T_{TI}	T_{L2}	$T_{T\&P}$	$T_{F\&H}$	T_{VDV}	T_{CHIN}
GC	SS1	5.0	1.0	401	600	551	579	889	953	943	960	1107	1114
	SS2	7.5	1.0	1119	1350	1521	1563	1602	1623	1704	1660	1755	1790
	SS3	10.0	1.0	1208	1920	2173	2179	2314	2406	2439	2554	2640	2677
	SS4	7.5	1.0	1215	980	1430	1591	1657	1683	1727	1722	1820	1858
	SS5	7.5	1.0	1003	1280	1343	1374	1410	1444	1528	1541	1600	1626
	SS6	5.0	1.0	494	720	811	891	945	960	973	965	1020	1042
	SS7	10.0	1.0	1328	1800	1815	1819	1870	2090	2004	2343	2327	2379
	SS8	7.5	1.5	1406	1960	1956	2031	2193	2245	2307	2423	2520	2574
	SS9	7.5	1.5	1659	2240	2299	2338	2499	2574	2638	2829	2880	2931
	SS10	7.5	1.5	1382	1920	2062	2125	2202	2249	2347	2492	2560	2600
	SS11	5.0	1.5	842	840	1021	1039	1097	1126	1195	1260	1400	1414
	SS12	10.0	1.5	1779	2520	2930	2988	3235	3369	3400	3732	3780	3821
DC	SS13	3.5	1.0	297	300	316	332	341	351	377	353	400	415
	SS14	5.0	1.0	500	500	526	539	544	551	578	552	600	613
	SS15	7.5	1.0	770	900	940	933	978	1001	1058	1034	1100	1130
YC	SS16	5.0	1.0	346	400	415	417	438	451	463	428	500	503
	SS17	7.5	1.0	725	770	786	788	826	840	855	825	875	909
	SS18	10.0	1.0	903	945	970	978	1026	1052	1068	1057	1155	1176

[a] Interpreted uplift resistance for the various methods: T_{DB}, Debeer method; T_{DA}, Davisson method; T_{ST}, Slope tangent method; T_{TI}, Tangent intersection method; T_{L1}, L_1 method; T_{L2}, L_2 method; $T_{T\&P}$, Terzaghi and Peck method; $T_{F\&H}$, Fuller and Hoy method; T_{VDV}, Van der Veen method; T_{CHIN}, Chin method

Table 3 Dimensions and interpreted uplift resistances for the belled shafts

Site	Shaft No.	Shaft and bell geometry				Interpreted uplift resistance, T [a] (kN)									
		D (m)	b (m)	B (m)	θ (°)	T_{L1}	T_{DB}	T_{DA}	T_{ST}	T_{TI}	T_{L2}	$T_{T\&P}$	$T_{F\&H}$	T_{VDV}	T_{CHIN}
	BS1	1.8	0.9	1.2	15	102	275	274	269	273	278	284	251	300	303
	BS2	2.9	1.2	1.9	30	467	540	937	943	1075	1088	1099	1082	1170	1191
	BS3	4.1	1.5	2.7	45	1256	1250	1875	2037	2448	2530	2540	2636	2750	2826
	BS4	3.0	1.2	1.5	15	332	425	522	581	769	853	798	802	941	943
	BS5	4.4	1.5	2.2	30	1166	1380	1580	1638	2068	2332	2321	2744	2784	2835
GC	BS6	4.2	0.9	2.1	45	987	1140	1238	1319	1499	1700	1587	1810	2093	2167
	BS7	4.5	1.5	1.8	15	816	1400	1361	1403	1526	1616	1624	1688	2026	2166
	BS8	4.0	0.9	1.6	30	626	900	922	943	1108	1205	1193	1218	1352	1364
	BS9	6.0	1.2	2.4	45	1304	2160	2263	2422	2864	3524	3067	3752	3725	3815
	BS10	7.5	1.0	2.0	40	1086	1750	1733	1814	2355	2450	2550	3389	3516	3521
	BS11	7.5	1.5	3.0	45	1330	3000	2114	2640	3090	3631	3815	5400	5575	5874
	BS12	3.5	1.0	2.0	40	365	700	532	592	755	803	811	812	901	935
DC	BS13	5.0	1.0	2.0	40	809	1000	1065	1144	1366	1510	1436	1531	1612	1639
	BS14	7.5	1.0	2.0	40	1077	1600	1621	1643	1925	2227	2340	2316	2413	2593
YC	BS15	7.5	1.0	2.0	40	616	1120	1033	1071	1199	1250	1278	1286	1400	1412

[a] Interpreted uplift resistance for the various methods: T_{DB}, Debeer method; T_{DA}, Davisson method; T_{ST}, Slope tangent method; T_{TI}, Tangent intersection method; T_{L1}, L_1 method; T_{L2}, L_2 method; $T_{T\&P}$, Terzaghi and Peck method; $T_{F\&H}$, Fuller and Hoy method; T_{VDV}, Van der Veen method; T_{CHIN}, Chin method.

to the required depth and diameter, which was identical to the construction of the straight-sided shafts. Then, the second step was conducted to enlarge the circular base to the required dimensions. During the excavating, the diameter and the verticality of each shaft were measured at an interval of approximately 1 m until the required depth was achieved. All of the dimensional values in Tables 2 and 3 are the means of the measured data, and all foundation shafts had truly vertical faces.

4. Loading procedure and test method

Each of the load tests was conducted after the concrete had cured for approximately 28 days. All of the tests were conducted with static monotonic loading and without cycling. The same loading, reaction, instrumentation, and data acquisition systems were used for all tests.

The test set-up was designed according to the criteria recommended in CEI/IEC 1773 (CEI/IEC 1996), as shown in Fig. 6. As may be seen from Fig. 6, the tested shaft was axially loaded, and the reaction beams were placed perpendicular to the concrete supporting blocks. The clear distance between the reaction concrete blocks was 10 m and would be relatively far away to avoid affecting the test results. During each of the tests, four electronic displacement sensors were placed at the four points on the shaft head with a-90°-separation. All of the sensors were attached to the

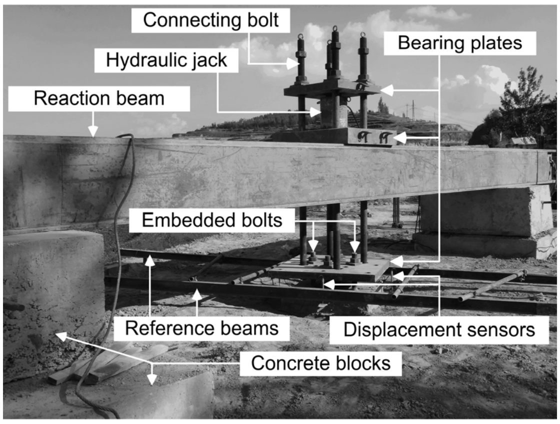

Fig. 6 Test set-up for uplift loading

reference beams installed over the top plane of the shaft. The reference beams were sufficiently stiff to support the instrumentation and prevent excessive variations in the readings.

The slowly maintained load method was adopted for all tests, i.e., the uplift loading was applied in a load increment of 10% of the predicted axial uplift resistance of each individual foundation, and the foundation was allowed to move under each maintained-load increment until a certain rate of displacement was achieved. Each load increment was maintained after loading until two consecutive displacements within each hour were less than 0.1 mm. The next load increment was then added. The pullout test was continued to the point of failure. The foundation was then unloaded by removing the test load. This is the typical test procedure recommended in Chinese National Standard GB50007-2011 (CNS 2011) and Chinese Local Standard JGJ 94-2008 (CLS 2008).

5. Load test results and analysis

5.1 Interpretation of load tests

In this study, the uplift load test results of the straight-sided and belled shafts were discussed in terms of load–displacement curves. Appendix A illustrates the plots that relate the applied uplift load to the average shaft head displacement for each of the straight-sided and belled shafts.

As may be seen from Appendix A, the uplift load versus shaft head displacement curves for the straight-sided and belled shafts approximately exhibited an initial linear, a curvilinear transition, and a final linear region. In general, the load–displacement curves obtained from the uplift loads test did not provide a well-defined peak or asymptotic value of the load; therefore, estimating the uplift failure load needed to be interpreted as done in the previous studies (Akbas and Kulhawy 2009, Briaud 2007, Chen 2004, Chen and Chu 2012, Chen and Fang 2009, Chen and Lee 2010, Chen *et al*. 2008, 2011, Marcos *et al*. 2013, Qian *et al*. 2014b). The nine interpretation criteria shown in Table 4 were used to interpret the failure load or resistance from the uplift load versus shaft head displacement curve of each load test. These criteria employ varied interpretation bases as noted in Table 4, and they represent a wide distribution of interpreted results from the lower, middle, and higher bounds as found in practices.

Table 4 Definitions of representative uplift interpretation criteria

Method	Category	Definition of interpreted uplift resistance
Van der Veen (1953)	Mathematical model	T_{VDV} is P_{ult} that gives a straight line when log $(1\text{-}P/P_{ult})$ is plotted versus total displacement
Chin (1970)	Mathematical model	T_{CHIN} is equal to the inverse slope, 1/m, of the line, $s/T = \mathrm{m}s + \mathrm{c}$, where T is the uplift load, s is the total displacement, and m, c is the slope and intercept of the line, respectively.
Terzaghi and Peck (1967)	Settlement limitation	$T_{T\&P}$ is the load that occurs at 1.0 in. (25.4 mm) total displacement.
Fuller and Hoy (1970)	Settlement limitation	$T_{F\&H}$ is the minimum load that occurs at a rate of total displacement of 0.05 in. per ton (0.14 mm/kN).
DeBeer (1970)	Settlement limitation	T_{DB} is the load at the change in slope on a log–log total displacement curve.
Davisson (1972)	Settlement limitation	T_{DA} occurs at a displacement equal to the shaft elastic uplift line, PD/EA, offset by 0.15 in. (3.8 mm), where P = uplift load, D = depth, A = area, and E = Young's modulus.
Slope tangent (O'Rourke and Kulhawy 1985)	Graphical construction	T_{ST} occurs at a displacement equal to the initial slope of the load–displacement curve plus 0.15 in. (3.8 mm).
Tangent intersection (Housel 1966, Tomlinson 1977)	Graphical construction	T_{TI} is determined as the intersection of two lines drawn as tangents to the initial linear and final linear portions of the load–displacement curve and projected to the load – displacement curve.
L_1–L_2 (Hirany and Kulhawy 1988, 1989, 2002)	Graphical construction	T_{L1} and T_{L2} correspond to elastic limit and failure threshold loads, respectively, as shown in Fig. 7.

The definitions of interpreted failure load or resistance by Van der Veen (1953) and Chin (1970) are based on mathematical models that correspond to the asymptote of the load–displacement curve. The interpreted capacities by Terzaghi and Peck (1967) and Fuller and Hoy (1970) are defined as the load at an absolute displacement and a rate of displacement, respectively, while DeBeer (1970), which is also based on a displacement limit, determines the uplift resistance at the load occurring in the change of slope from the log-log plot of the total load–displacement curve. The Davisson method (1972) is a graphical construction and defines the uplift resistance at the intersection of the load–displacement curve and the shaft elastic uplift line offset by 3.8 mm. The slope tangent method (O'Rourke and Kulhawy 1985) is a modification of the Davisson method (Davisson 1972) and uses the initial slope instead of the elastic line. The failure load is determined from the intersection of a line drawn parallel to the initial linear portion of the load–displacement curve at a distance equivalent to a displacement of 3.8 mm. The tangent intersection method (Housel 1966, Tomlinson 1977) has also been used to interpret the failure load, which is determined as the intersection of two lines drawn as tangents to the initial linear and final linear portions of the load–displacement curve. The L_1–L_2 method (Hirany and Kulhawy 1988, 1989, 2002) is based on the fact that a load–displacement curve can generally be simplified into three

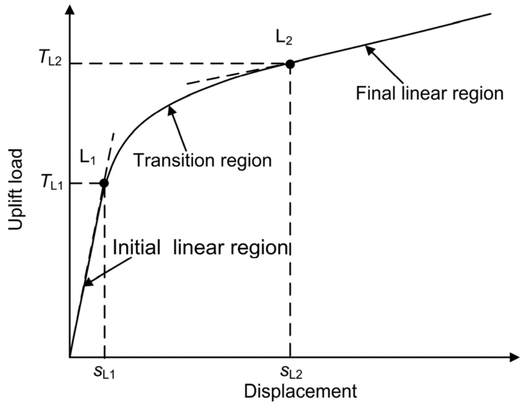

Fig. 7 Sectors of load–displacement curve for L_1–L_2 method (Hirany and Kulhawy 1988)

distinct sectors: initial linear, non-linear curve transition, and final linear, as illustrated in Fig. 7. Point L_1 (elastic limit) corresponds to the load (T_{L1}) and displacement (s_{L1}) at the end of the initial linear region, whereas L_2 (failure threshold) corresponds to the load (T_{L2}) and displacement (s_{L2}) at the beginning of the final linear region.

Tables 2 and 3 show the interpreted uplift resistances for the straight-sided and belled shafts, respectively. Appendix B presents the displacements at the interpreted criteria. Comparisons of the uplift resistances in Tables 2 and 3 for the straight-sided and belled shafts indicated that the belled shafts generally had higher uplift resistances than the straight-sided shafts with the same dimensions of *D* and *b*. This difference should be attributed to with bell and without bell. The belled shafts can effectively mobilize the shear resistance of the soil above the enlarged base and are thus superior to the straight-sided shafts.

5.2 Comparison of straight-sided and belled shafts in loess

In this study, the failure threshold, T_{L2}, of the L_1-L_2 method was adopted as a base for comparing the interpretation criteria, and all of the interpreted uplift resistances were normalized by T_{L2} for two reasons. First, the L_1-L_2 method could interpret all the load test cases, and second, T_{L2} can be generally defined as the "interpreted failure load" or "interpreted resistance" because, beyond T_{L2}, a small increase in load gives a significant increase in displacement. Therefore, the results below were compared to evaluate the interrelationships and characteristics of the methods. T_{L1} was included for reference only. It is neither an interpreted failure load nor a capacity but rather an elastic limit.

The statistics for the interpreted uplift resistances of the straight-sided and belled shafts are summarized in Tables 5, including the minimum, maximum, mean, standard deviation (SD), and coefficient of variation (COV) of the interpreted results. Table 6 presents the summary comparisons of the interpreted displacements at the interpreted criteria for the straight-sided and belled shafts, including the mean, SD, and COV values of the interpreted results.

The results in Tables 5 show mean interpreted load ratios ranging from 0.82 to 1.13 for straight-sided shafts and 0.71 to 1.20 for belled shafts when compared to T_{L2}, with COV value of 0.02 to 0.12 (straight-sided) and 0.05 to 0.22 (belled). The general trends of mean ratios for the straight-sided and belled shafts in the loess are similar, and the COV values are comparable.

Table 5 Summary of the interpreted uplift resistance ratios

Foundation type	Statistics	Interpreted uplift resistance ratio, T/T_{L2}								
		T_{L1}	T_{DB}	T_{DA}	T_{ST}	T_{TI}	$T_{T\&P}$	$T_{F\&H}$	T_{VDV}	T_{CHIN}
Straight-sided shafts	Minimum	0.42	0.58	0.58	0.61	0.89	0.96	0.95	1.04	1.08
	Maximum	0.91	0.92	0.95	0.98	0.99	1.07	1.12	1.24	1.26
	Mean	0.69	0.82	0.89	0.91	0.97	1.03	1.04	1.11	1.13
	SD	0.14	0.10	0.08	0.08	0.02	0.03	0.05	0.04	0.04
	COV	0.20	0.12	0.09	0.09	0.02	0.03	0.05	0.04	0.04
Belled shafts	Minimum	0.37	0.49	0.58	0.68	0.81	0.87	0.90	1.05	1.08
	Maximum	0.58	0.99	0.99	0.97	0.99	1.05	1.49	1.54	1.61
	Mean	0.46	0.71	0.74	0.78	0.92	0.99	1.08	1.17	1.20
	SD	0.07	0.16	0.11	0.08	0.05	0.05	0.16	0.14	0.15
	COV	0.14	0.22	0.14	0.10	0.06	0.05	0.15	0.12	0.13

Table 6 Summary comparisons of the interpreted displacements

Foundation type	Statistics	Displacement at the interpreted criteria, s^{a} (mm)								
		s_{L1}	s_{DB}	s_{DA}	s_{ST}	s_{TI}	s_{L2}	$s_{F\&H}$	s_{VDV}	s_{CHIN}
Straight-sided shafts	Mean	1.12	2.42	4.34	5.66	10.10	13.69	32.33	>61.65	>62.83
	SD	0.58	1.15	0.38	0.79	3.75	7.14	21.52	14.89	14.71
	COV	0.52	0.48	0.09	0.14	0.37	0.52	0.67	0.24	0.23
Belled shafts	Mean	1.11	4.33	4.33	5.51	14.29	25.75	46.37	>76.13	>76.25
	SD	0.48	2.62	0.35	0.78	3.97	11.59	27.02	12.46	12.63
	COV	0.43	0.60	0.08	0.14	0.28	0.45	0.58	0.16	0.17

[a] by definition, $s_{T\&P}$ = 25.4 mm, and there is no statistics

However, for all of the criteria, there were somewhat smaller mean ratio values for the straight-sided shafts. Among these methods, T_{DB} is the lowest mean interpreted ratio and presents a higher COV among all interpretation criteria. The T_{L1} has the smallest mean ratio and displacement (Table 6), which implies that the initial linear region occurs within a very small displacement. The statistics of the mean ratios show that smaller interpreted uplift resistances and displacements correspond to higher COVs. This phenomenon has also been observed by Chen and Chu (2012) and by Marcos *et al*. (2013), which may result from fluctuation during the initial loading or possible measurement sensitivity.

The mean uplift displacements for the straight-sided and belled shafts shown in Table 6 follow the same order trend as the uplift resistances. For the straight-sided shafts, the displacements at the interpreted failure load ranged from 2.42 mm at T_{DB} to 4.34 mm at T_{DA} to 13.69 mm at T_{L2} to greater than (>) 62.83 mm at T_{CHIN}, while the belled shafts ranged from 4.33 mm at T_{DB} and T_{DA} to 25.75 mm at T_{L2} to greater than (>) 76.25 mm at T_{CHIN}. The COV values for these displacement data were high with a range of 0.09 to 0.67 (straight-sided) and 0.08 to 0.60 (belled).

To examine more general foundation behaviors, the normalized uplift load–displacement curves for the straight-sided and belled shafts are presented in Fig. 8 as plots that relate the mean ratio of

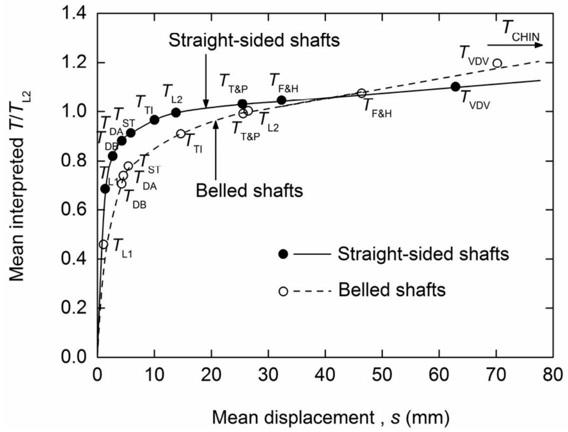

Fig. 8 Mean load–displacement comparison of straight-sided and belled shafts in the loess

each interpreted resistance to T_{L2} against the mean shaft-head-displacement at the corresponding interpreted load. Comparisons of the straight-sided and belled shafts in Fig. 8 show some interesting features.

First, overall similar general trends are observed by the interpreted results of all criteria for the straight-sided and belled shafts in the loess. The Debeer, Davisson, slope tangent, and tangent intersection methods are typically located within the L_1 to L_2 non-linear transition region of the load–displacement curve, and the Terzaghi and Peck method is close to the failure threshold T_{L2}, while Fuller and Hoy and Van der Veen are beyond the failure threshold T_{L2} but are generally lower than T_{CHIN}. Therefore, defining the failure load as T_{CHIN} results in values that are overly high, likely because T_{CHIN} is based on a mathematical model that corresponds to the asymptote of the load–displacement curve. This conclusion is consistent with the results that have been observed in the evaluations of both axial uplift and compression interpretation criteria (Akbas and Kulhawy 2009, Chen 2004, Chen and Chu 2012, Chen and Fang 2009, Chen *et al*. 2008, Marcos *et al*. 2013, Qian *et al*. 2014b).

Second, prior to the failure threshold point L_2 corresponding to the load T_{L2}, the mean displacements of all interpretation criteria for belled shafts are clearly greater than those for straight-sided shafts in general. This difference should be related to the differences in the foundation types and the failure mechanisms. The straight-sided shafts without a bell get uplifted both by shearing at the shaft-soil contact and through the surrounding soil, and a composite failure surface may develop. In general, the uplift resistance of the straight-sided shafts in the loess is mainly derived and determined by the shear strength along the soil-shaft interface, and the full resistance would be mobilized when the shear strength along the soil-shaft interface is fully developed. However, for the belled shafts, they can effectively mobilize the shear resistance of the undisturbed soil above the enlarged base. The uplift resistance of the belled shafts in uplift would be mainly determined by the shearing resistance along the soil-soil failure interface, the dead weight of the foundation, and the weight of the soil within the truncated breakout region. The failure zone for the belled shafts in uplift is mainly the soil-soil interface along the circumference of the breakout region, and the tendency of the loess to dilate becomes significant when the bell is subjected to the uplift loading. Therefore, the displacement required to completely mobilize the uplift resistance would be greater.

5.3 Comparison of straight-sided shafts in different soils

Fig. 9 shows the comparisons of uplift load–displacement curves of the straight-sided shafts for different soils. The results were collected from Chen *et al*. (2008) for cohesive soils, Chen and Chu (2012) for gravelly soils, and Qian *et al*. (2014b) for Gobi gravel soils. For ease in comparison, L_1 and L_2 are also marked in Fig. 9.

As shown in Fig. 9, the interpreted results of all criteria for the straight-sided shafts in different soils display similar trends. However, prior to the uplift failure threshold of T_{L2}, the mean displacements of all interpretation criteria for straight-sided shafts in the loess are generally lower than those in the cohesive, gravelly, and Gobi gravel soils. Beyond the end of the transition region, the mean displacements for straight-sided shafts in the loess are larger than those in the cohesive soils. Chen and Chu (2012) noted that the greater mean displacements of all interpretation criteria for drilled shafts in gravelly soils are larger than those in non-gravelly soils may be due to the somewhat irregular shaft shape existing in the gravel excavation. The irregular shaft shape increases the roughness of the soil-shaft interface, and the tendency of gravel to dilate becomes significant when the shaft is subjected to uplift loading. Therefore, a greater displacement is required to completely mobilize the uplift capacity. Qian *et al*. (2014b) pointed out that the irregular shaft shape of the foundation and the salt cementation of the Gobi gravel would be the reason that the mean displacements for straight-sided shafts in the Gobi gravel are larger than those in the cohesive soils. Therefore, this may also be the reason that the mean displacements for the straight-sided shafts in the loess soil are lower than those in the gravelly and Gobi gravel soils prior to the failure threshold T_{L2}.

The phenomenon of which the mean displacements for straight-sided shafts in the loess are lower than those in the cohesive soils prior to the failure threshold T_{L2} but greater than those in the cohesive soils beyond the end of the transition region may be due to the difference in the foundation dimension. The depth-to-diameter ratios of the drilled shafts ranged from 1.6 to 56.0 in cohesive soils (Chen *et al*. 2008). However, the corresponding ratios for the straight-sided shafts discussed in this study ranged from 3.3 to 10.0. According to the previous studies (Pacheco *et al*. 2008), the straight-sided shafts in this study would mainly be in a shallow failure mode, while most of the drilled shafts discussed by Chen *et al*. (2008) were primarily in a deep failure mode.

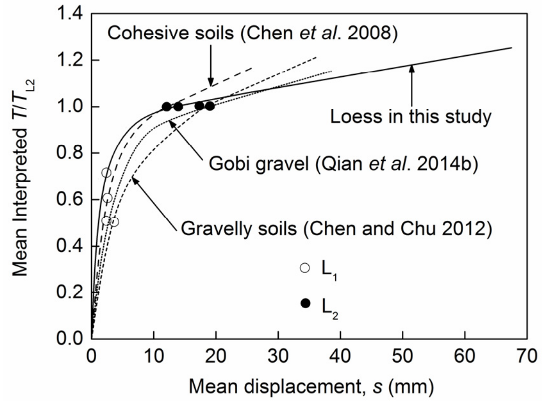

Fig. 9 Comparison of uplift load–displacement curves of straight-sided shafts for different soils

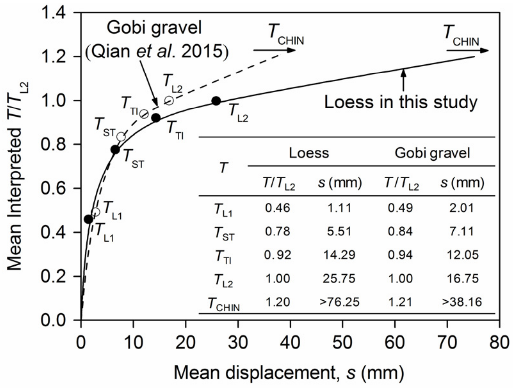

Fig. 10 Comparison of uplift load–displacement curves of belled shafts for different soils

5.4 Comparison of belled shafts in loess and Gobi gravel soils

Based on the results of forty-one full-scale uplift load tests on belled shafts at seven Gobi gravel sites in Northwest China, Qian *et al*. (2015) evaluated the uplift performance of belled shafts in Gobi gravel by four representative interpretation criteria (Chin, Slope tangent, Tangent intersection, and L_1–L_2), and the results were interrelated to establish a generalized correlation among these interpreted uplift resistances using a mean normalized uplift load-displacement curve.

Fig. 10 shows a comparison between the normalized uplift load–displacement relationship of belled shafts in loess and Gobi gravel soils. For ease of observation, the corresponding ratio of four interpretation method to T_{L2} and its displacement are also shown.

First, overall similar general trends are observed by the interpreted results of four criteria for the belled shafts in the loess and Gobi gravel. The slope tangent method gives the lowest values, while the Chin method yields the highest values and always lies above T_{L2}. The slope tangent and tangent intersection methods yield ratio values less than 1.0, and are therefore located in the nonlinear transition between L_1 and L_2.

Second, it is clear that, prior to the interpreted uplift resistance of T_{ST}, the mean load–displacement curves for the belled shafts in the loess and Gobi gravel soils are comparable. However, beyond the uplift resistance of T_{ST}, the load–displacement relationship for the belled shafts in the Gobi gravel shows a substantially stiffer load–displacement response than that in the loess. This indicates that the Gobi soil stiffness is much greater than that of the loess soil. This difference should be related to the consequence of subtle differences in the soils. As described by Qian *et al*. (2014b, 2015), Gobi gravel contains some soluble salts. The precipitation of the dissolved salts may have resulted in salt cementation of the particulate soil matrix in Gobi gravel. Therefore, under dry environment, Gobi gravel has a high uplift capacity and low compressibility. According to the direct shear tests, the ranges of the internal friction angle of Gobi gravel were 40.6-43.6°, compared to less than 40° for the loess described in this paper. As a result, the Gobi soil stiffness is much greater than that of the loess soil.

6. Design recommendations

Based on the data analyses of the straight-sided and belled shafts in the loess, the interpretation

Table 7 Summary of the uplift resistance approximations using L_1 as a reference

Foundation type	Interpreted uplift resistance ratio, T/T_{L1}								
	T_{DB}	T_{DA}	T_{ST}	T_{TI}	T_{L2}	$T_{T\&P}$	$T_{F\&H}$	T_{VDV}	T_{CHIN}
Straight-sided shafts	1.23	1.33	1.37	1.47	1.52	1.56	1.59	1.70	1.72
Belled shafts	1.57	1.63	1.72	2.02	2.21	2.19	2.39	2.60	2.61

criteria can be classified into four groups to determine a reasonable ultimate uplift resistance based on their statistical results. (i) The result of Chin's criterion is always above the measured load–displacement curve and will not be conservative. However, Chin's interpretation method is straightforward and less subjective. (ii) The L_2, Terzaghi and Peck, Fuller and Hoy, and Van der Veen criteria have nearly identical mean interpreted results. These four criteria present the same reliability. (iii) The DeBeer, Davisson, slope tangent, and tangent intersection methods yield interpreted T/T_{L2} ratios less than 1.0; therefore, these four criteria are located in the nonlinear transition between L_1 and L_2. (iv) The L_1 criterion occurs at very small displacements (< 5 mm).

For the above analyses, the L_1-L_2 method is generally preferred for interpreting the uplift resistance because it is based on the failure threshold load and considers the shape of the load-displacement curve and the ratio of the change in load to the change in displacement. Therefore, the L_1 method would be suitable for the design of serviceability limit state (SLS) conditions (dealing with foundation displacement) because the initial part of a load-displacement curve will have an important design significance in practice. As illustrated in Fig. 7, point L_1 in the L_1–L_2 method is also a convenient reference point because it corresponds to the elastic limit load at the end of the initial linear region within the curve. As a result, it would be useful in demonstrating the general relationships among the interpretation criteria and providing uplift resistance approximations. Using L_1 as a reference, the uplift resistance approximations for uplift resistances of the straight-sided and belled shafts were listed in Table 7. First, these uplift resistance approximations could be used with caution to interrelate the interpretation criteria when necessary to address insufficient load–displacement data. Second, the practical implication of these uplift resistance approximation values is that, on average, a safety factor between 2 and 3 should be implemented to ensure that the foundation resistance of a straight-sided or belled shaft may be within the elastic limit in most designs.

However, the other criteria could also be applied for the design of ultimate limit state (ULS) conditions (dealing with foundation resistance) based on the requirements of structure type. The Debeer, Davisson, Slope tangent, Tangent intersection, and L_2 methods give mean interpreted "failure" displacements from 2 mm to 25 mm. At the elastic limit L_1, the mean interpreted displacement is 1.12 mm for straight-sided shafts and 1.11 mm for belled shafts, respectively. For most designs, a settlement of 25 mm could be allowable for most routine building structures (Dithinde *et al*. 2011). Therefore, using the Debeer, Davisson, Slope tangent, Tangent intersection, and L_2 methods as the definition for interpreted failure load, with a minimum safety factor of 2, the mean displacement would be close to the amount of L_1 and will be close to the elastic behavior.

It should be noted that the results and design recommendations shown in this study are general behaviors applicable for the straight-sided and belled shafts in the loess only, and any extrapolation of these results to other different soils and foundations is not recommended.

7. Conclusions

The following conclusions can be derived based on the comparative field uplift tests on 18 straight-sided and 15 belled shafts at the three collapsible loess sites under an arid environment:

(1) Relatively different shapes of the load–displacement curves occurred for the straight-sided and belled shafts, but these load–displacement curves approximately exhibited an initial linear, a curvilinear transition, and a final linear region, and the uplift resistance should be defined by an "interpreted failure load" using an appropriate criterion, as done in other studies. In general, at the same loess site, the belled shafts had higher uplift resistances than the straight-sided shafts with the same shaft diameter and length.

(2) The interpreted uplift failure load results for the nine interpretation criteria (Van der Veen, Chin, Terzaghi and Peck, Fuller and Hoy, DeBeer, Davisson, Slope tangent, Tangent intersection, and L_1–L_2) generally presented the same trend for the straight-sided and belled shafts in the loess. Of these, the Debeer method gave the lower bound, while the Chin method was the upper bound. The Debeer, Davisson, slope tangent, and tangent intersection methods were typically located within curvilinear transition region of the load–displacement curve, while Terzaghi and Peck, Fuller and Hoy, and van der Veen are close to and beyond the failure threshold T_{L2} but are generally lower than T_{CHIN}.

(3) Comparisons of the normalized load–displacement curves for the straight-sided and belled shafts in the loess indicated that, prior to the failure threshold point L_2 corresponding to the load T_{L2}, the mean displacements of all interpretation criteria for belled shafts are generally greater than those for straight-sided shafts. This difference should be related to the differences in the foundation types and the failure mechanisms. The displacement required to completely mobilize the uplift resistance for the belled shafts would be larger.

(4) A safety factor between 2 and 3 should be implemented to ensure that the uplift resistance of a straight-sided or belled shaft will be within the elastic limit. When using the Debeer, Davisson, Slope tangent, Tangent intersection, and L_2 methods as the definition for interpreted failure load, with a minimum safety factor of 2, the mean displacement would be close to the amount of L_1 and close to elastic behavior in most designs.

Acknowledgments

The author wish to thank the State Grid Corporation of China for the support of the projects (No. GCB17201200123, No. GCB17201200089). The authors also appreciate the reviewers' excellent comments, which have improved the quality of this paper.

References

Akbas, S.O. and Kulhawy, F.H. (2009), "Axial compression of footings in cohesionless soils. I: Load–settlement behavior", *J. Geotech. Geoenviron. Eng.*, **135**(11), 1562-1574.

Assallay, A.M., Rogers, C.D.F. and Smalley, I.J. (1996), "Engineering properties of loess in Libya", *J. Arid. Environ.*, **32**(4), 373-386.

ASTM (2007), Standard test method for particle-size analysis of soils, ASTM D422-63, American Society for Testing and Materials. ASTM International, West Conshohocken, PA, USA.

ASTM (2011a), Standard practice for classification of soils for engineering purposes (Unified Soil

Classification System), ASTM D2487-11; American Society for Testing and Materials, ASTM International, West Conshohocken, PA, USA.

ASTM (2011b), Standard test method for direct shear test of soils under consolidated drained conditions, ASTM D3080/D3080M-11; American Society for Testing and Materials, ASTM International, West Conshohocken, PA, USA.

Briaud, J.L. (2007), "Spread footings in sand: Load settlement curve approach", *J. Geotech. Geoenviron. Eng.*, **133**(8), 905-920.

CEI/IEC (1996), Overhead lines-Testing of foundation for structures, CEI/IEC 1773; Commission Electrotechinque Internationale/International Electrotechnical Commission, Bureau central de la Commission Electrotechnique Internationale 3, Geneva, Switzerland.

Chen, J.R. (2004), "Axial behavior of drilled shafts in gravelly soils", Ph.D. Thesis; Department of Civil and Environmental Engineering, Cornell University, New York, NY, USA.

Chen, Y.J. and Chu, T.H. (2012), "Evaluation of uplift interpretation criteria for drilled shafts in gravely soils", *Can. Geotech. J.*, **49**(1), 70-77.

Chen, Y.J. and Fang, Y.C. (2009), "Critical evaluation of compression interpretation criteria for drilled shafts", *J. Geotech. Geoenviron. Eng.*, **135**(8), 1056-1069.

Chen, Y.J and Lee, Y.H. (2010), "Evaluation of lateral interpretation criteria for drilled shaft capacity", *J. Geotech. Geoenviron. Eng.*, **136**(8), 1124-1136.

Chen, Y.J., Chang, H.W. and Kulhawy, F.H. (2008), "Evaluation of uplift interpretation criteria for drilled shaft capacity", *J. Geotech. Geoenviron. Eng.*, **134**(10), 1459-1468.

Chen, Y.J., Lin, S.W. and Kulhawy, F.H. (2011), "Evaluation of lateral interpretation criteria for rigid drilled shafts", *Can. Geotech. J.*, **48**(4), 634-643.

Chin, F.K. (1970), "Estimation of the ultimate load of piles not carried to failure", *Proceedings of the 2nd Southeast Asian Conference on Soil Engineering*, Singapore, June, pp. 81-90.

CLS (2008), Technical code for building pile foundations, Chinese Local Standard JGJ 94-2008; China Architecture and Building Press, Beijing, China. [In Chinese]

CNS (2011), Code for design of building foundations, Chinese National Standard GB50007-2011; China Architecture and Building Press, Beijing, China. [In Chinese]

Davisson, M.T. (1972), "High capacity piles", *Proceedings of the Lecture Series on Innovations in Foundation Construction*, ASCE, Illinois Section, Chicago, IL, USA, March, pp. 81-112.

DeBeer, E.E. (1970), "Experimental determination of the shape factors and bearing capacity factors of sand", *Géotechnique*, **20**(4), 387-411.

Derbyshire, E., Meng, X.M., Wang, J.T., Zhou, Z.Q. and Li, B.X. (1995), "Collapse loess on the Loess Plateau of China", In: *Genesis and Properties of Collapsible Soils* (E. Derbyshire, T. Dijkstra and I.J. Smalley Eds.), Kluwer, Dordrecht, The Netherlands, pp. 267-293.

Dithinde, M., Phoon, K.K., Wet, M.D. and Retief, J.V. (2011), "Characterization of model uncertainty in the static pile design formula", *J. Geotech. Geoenviron. Eng.*, **137**(1), 70-85.

Fuller, F.M. and Hoy, H.E. (1970), "Pile load tests including quick load test method, conventional methods, and interpretations", Highway Research Board, Research Record 333; Washington, D.C., USA, pp. 74-86.

Gao, G.R. (1988), "Formation and development of the structure of collapsing loess in China", *Eng. Geol.*, **25**(2-4), 235-245.

Hirany, A. and Kulhawy, F.H. (1988), "Conduct and interpretation of load tests on drilled shaft foundations: Detailed guidelines", Report No. EPRI EL-5915; Electric Power Research Institute, Palo Alto, CA, USA, pp. 272-273.

Hirany, A. and Kulhawy, F.H. (1989), "Interpretation of load tests on drilled shafts. II: Axial uplift", In: *Foundation Engineering: Current Principles and Practices* (F.H. Kulhawy Eds.), New York, NY, USA, pp. 1150-1159.

Hirany, A. and Kulhawy, F.H. (2002), "On the interpretation of drilled foundation load test results", In: *Deep Foundations* (M.W. O'Neill and F.C. Townsend Eds.), *ASCE*, Reston, VA, USA, pp. 1018-1028.

Housel, W.S. (1966), "Pile load capacity: Estimates and test results", *J. Soil Mech. Found. Div.*, **92**(SM4), 1-30.

Hwang, H., Wang, L. and Yuan, Z. (2000), “Comparison of liquefaction potential of loess in Lanzhou, China, and Memphis, USA”, *Soil Dyn. Earthq. Eng.*, **20**(5-8), 389-395.
Kulhawy, F.H., Trautmann, C.H., Beech, J.F., O’Rourke, T.D. and McGuire W. (1983), “Transmission line structure foundation for uplift-compression loading”, Report No. EPRI-EL-2870; Electric Power Research Institute, Palo Alto, CA, USA.
Liang, Q.G., Wu, X.Y., Li, C.Q. and Wang, L.L. (2014), “Mechanical analysis using the unconfined penetration test on the tensile strength of Q_3 loess around Lanzhou City, China”, *Eng. Geol.*, **183**, 324-329.
Marcos, M.C.M., Chen, Y.J. and Kulhawy, F.H. (2013), “Evaluation of compression load test interpretation criteria for driven precast concrete pile capacity”, *KSCE J. Civ. Eng.*, **17**(5), 1008-1022.
Nouaouria, M.S., Guenfoud, M. and Lafifi, B. (2008), “Engineering properties of loess in Algeria”, *Eng. Geol.*, **99**(1-2), 85-90.
O’Rourke, T.D. and Kulhawy, F.H. (1985), “Observations on load tests on drilled shafts”, *In Drilled piers and caissons II* (C.N. Baker Eds.), ASCE, New York, NY, USA, pp. 113-128.
Qian, Z.Z., Lu, X.L., Yang, W.Z. and Cui, Q. (2014a), “Behaviour of micropiles in collapsible loess under tension or compression load”, *Geomech. Eng., Int. J.*, **7**(5), 477-493.
Qian, Z.Z., Lu, X.L. and Yang, W.Z. (2014b), “Axial uplift behavior of drilled shafts in Gobi gravel”, *Geotech. Test. J.*, **37**(2), 205-217.
Qian, Z.Z., Lu, X.L., Han, X. and Tong, R.M. (2015), “Interpretation of uplift load tests on belled piers in Gobi gravel”, *Can. Geotech. J.*, **52**(7), 992-998.
Pacheco, M.P., Danziger, F.A.B. and Pinto, C.P. (2008), “Design of shallow foundations under tensile loading for transmission line towers: an overview”, *Eng. Geol.*, **101**(3-4), 226-235.
Ryashchenko, T.G., Akulovaa, V.V. and Erbaeva, M.A. (2008), “Loessial soils of Priangaria, Transbaikalia, Mongolia, and Northwestern China”, *Quaternary Int.*, **179**(1), 90-95.
Terzaghi, K. and Peck, R.B. (1967), *Soil Mechanics in Engineering Practice*, (2nd Ed.), Wiley, New York, NY, USA.
Tomlinson, M.J. (1977), *Pile Design and Construction Practice* (*A Viewpoint Publication)*, Cement & Concrete Association of Great Britain, London, UK.
Van der Veen, C. (1953), “Bearing capacity of a pile”, *Proceedings of the 3rd International Conference on Soil Mechanics and Foundation Engineering*, Zurich, Switzerland, August, International Society for Soil Mechanics and Geotechnical Engineering, London, UK. Vol. 2, pp. 85-90.
Wen, B.P. and Yan, Y.J. (2014), “Influence of structure on shear characteristics of the unsaturated loess in Lanzhou, China”, *Eng. Geol.*, **168**, 46-58.
Xu, L., Dai, F.C., Tu, X.B., Tham, L.G., Zhou, Y.F. and Iqbal, J. (2014), “Landslides in a loess platform, North-West China”, *Landslides*, **11**(6), 993-1005.
Yuan, Z.X. and Wang, L.M. (2009), “Collapsibility and seismic settlement of loess”, *Eng. Geol.*, **105**(1-2), 119-123.

CC

Appendix A

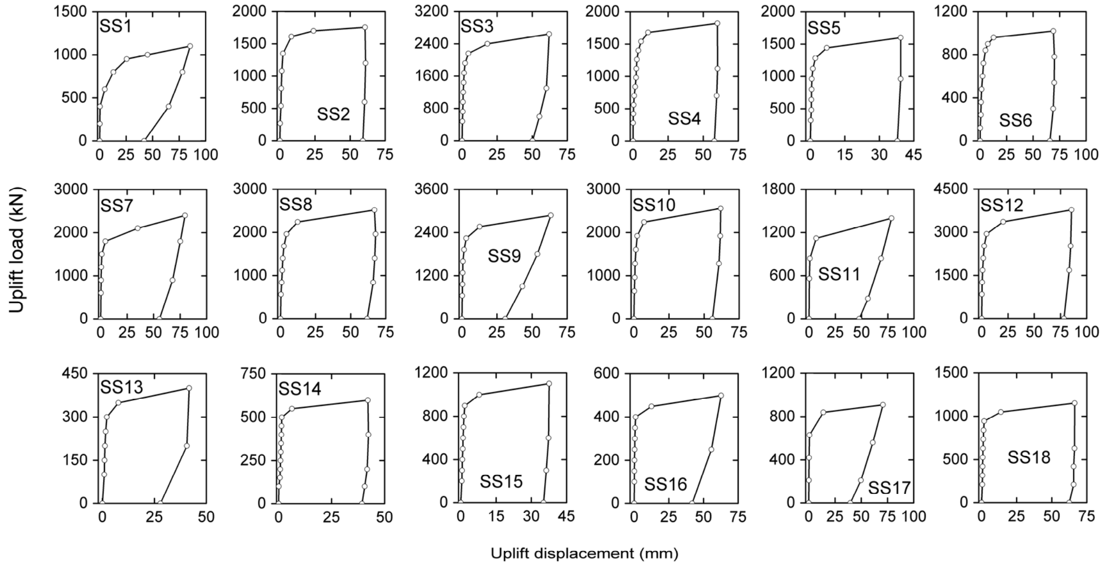

(a) Straight-sided shafts

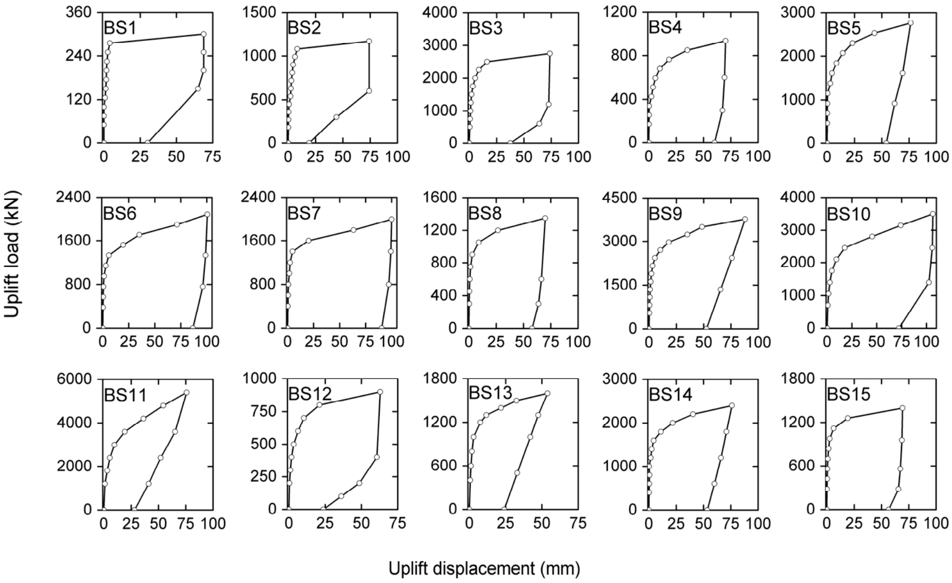

(b) Belled shafts

Fig. A Measured uplift load–displacement curves in field tests

Appendix B

Table B Summary of the interpreted displacements

Foundation type	Shaft No.	Displacement at the interpreted criteria [a, b] (mm)								
		s_{L1}	s_{DB}	s_{DA}	s_{ST}	s_{TI}	s_{L2}	$s_{F\&H}$	s_{VDV}	s_{CHIN}
Straight-sided shafts	SS1	0.25	4.84	3.78	4.31	20.4	26.28	30.65	> 85.47[c]	> 85.47[c]
	SS2	1.41	2.17	4.72	6.21	7.52	8.74	17.88	60.64	> 60.64[c]
	SS3	0.71	2.18	5.16	5.56	13.13	18.26	46.51	62.09	> 62.09[c]
	SS4	2.59	2.21	4.17	7.54	9.82	11.22	24.92	60.15	> 60.15[c]
	SS5	0.75	2.14	4.04	5.05	6.16	7.41	27.44	39.26	> 39.26[c]
	SS6	1.35	3.1	4.43	6.75	11.48	13.41	16.33	69.08	> 69.08[c]
	SS7	0.65	4.48	4.81	5.59	11.54	33.41	71.14	76.45	76.57
	SS8	1.59	4.32	4.32	6.27	10.88	12.94	47.33	66.98	> 66.98[c]
	SS9	0.86	3.12	4.11	5.57	10.77	13.5	55.4	63.41	> 63.41[c]
	SS10	0.96	2.35	4.61	5.53	6.78	7.87	49.11	61.86	> 61.86[c]
	SS11	0.71	0.78	4.86	5.17	6.41	7.48	42.64	78.57	> 78.57[c]
	SS12	0.95	2.31	4.56	6.21	15.55	21.29	77.67	85.54	> 85.54[c]
	SS13	2.06	2.15	3.95	6.29	7.39	9.07	11.12	41.74	> 41.74[c]
	SS14	1.41	1.51	3.86	5.33	5.63	7.01	11.23	42.11	> 42.11[c]
	SS15	1.22	1.66	4.15	5.27	6.48	8.14	16.81	37.58	> 37.58[c]
	SS16	0.52	1.03	4.29	4.84	9.66	12.86	8.74	62.77	> 62.77[c]
	SS17	0.68	1.29	4.12	4.66	11.24	13.92	10.82	49.55	70.71
	SS18	1.42	1.89	4.19	5.69	10.89	13.62	16.15	66.36	> 66.36[c]
Belled shafts	BS1	0.30	4.08	4.03	3.85	4.28	9.17	3.09	68.72	> 68.72[c]
	BS2	1.80	2.08	5.28	5.36	7.90	9.98	8.68	74.06	> 74.06[c]
	BS3	1.40	1.44	4.25	5.91	14.70	19.20	45.91	> 73.78[c]	> 73.78
	BS4	1.37	2.44	3.98	5.72	19.40	35.80	25.72	> 70.24[c]	> 70.24
	BS5	0.51	2.81	4.19	4.83	14.20	25.40	73.78	> 76.42[c]	> 72.65
	BS6	1.41	2.59	4.33	5.81	17.80	34.20	54.57	> 95.5[c]	> 96.57
	BS7	1.07	4.69	4.15	5.19	14.00	21.40	38.84	> 95.92[c]	> 95.29
	BS8	1.01	3.11	4.12	4.57	15.80	26.42	32.43	> 70.01[c]	> 70.00
	BS9	0.91	3.34	4.19	5.50	14.90	50.15	83.43	82.84	> 88.01[c]
	BS10	1.13	4.89	4.85	5.54	15.26	17.77	94.61	> 96.46[c]	> 96.46[c]
	BS11	1.41	9.71	4.23	7.17	11.16	19.71	75.87	> 75.87[c]	> 75.87[c]
	BS12	1.41	10.35	4.17	6.09	16.01	21.87	27.81	> 62.93[c]	> 62.93[c]
	BS13	1.82	2.97	4.36	6.12	17.87	33.19	40.03	> 53.85[c]	> 53.85[c]
	BS14	0.58	4.32	4.69	6.00	17.66	43.30	60.75	> 76.03[c]	> 76.03[c]
	BS15	0.45	6.20	4.07	5.05	13.42	18.76	30.05	69.26	> 69.26[c]

[a] Displacements for the various methods: s_{DB}, Debeer method; s_{DA}, Davisson method; s_{ST}, Slope tangent method; s_{TI}, Tangent intersection method; s_{L1}, L_1 method; s_{L2}, L_2 method; $s_{T\&P}$, Terzaghi and Peck method; $s_{F\&H}$, Fuller and Hoy method; s_{VDV}, Van der Veen method; s_{CHIN}, Chin method.

[b] by definition, $s_{T\&P}$ =25.4 mm, not included in the Table.

[c] the maximum displacement in the load test.